Gapless Kitaev Spin Liquid to Classical String Gas through Tensor Networks

Hyun-Yong Lee,[1] Ryui Kaneko,[1] Tsuyoshi Okubo,[2] and Naoki Kawashima[1,*]
[1]Institute for Solid State Physics, University of Tokyo, Kashiwa, Chiba 277-8581, Japan
[2]Department of Physics, University of Tokyo, Tokyo 113-0033, Japan

(Received 31 January 2019; published 23 August 2019)

We provide a framework for understanding the gapless Kitaev spin liquid (KSL) in the language of the tensor network (TN). Without introducing a Majorana fermion, most of the features of the KSL, including the symmetries, gauge structure, criticality, and vortex freeness, are explained in a compact TN representation. Our construction reveals a hidden string gas structure of the KSL. With only two variational parameters to adjust, we obtain an accurate KSL *Ansatz* with the bond dimension $D = 8$ in a compact form, where the energy is about 0.007% higher than the exact one.

DOI: 10.1103/PhysRevLett.123.087203

Introduction.—Quantum spin liquids represent a state of quantum matter which is not characterized by any local order parameters even at zero temperature. These novel states are expected to exhibit long-range entanglement leading to topological order and fractionalized excitations [1]. For example, nearest-neighbor resonating valence bond (NNRVB) states [2] have been extensively studied as variational wave functions for the ground states of frustrated quantum magnets [3,4]. Indeed, the NNRVB states are topologically ordered [3–7] and support spinon excitations carrying the fractionalized quantum number [4,5]. However, since they are not exact ground states of the antiferromagnetic Heisenberg model, variational methods with the NNRVB states have been employed to search for true ground states [8–11]. The Haldane phase, which is also known as the symmetry-protected topological phase, is another fascinating phase that one can find in the $S = 1$ quantum spin chain. The novel character that discriminates the Haldane phase from trivial gapped states was most clearly revealed by the discovery of the Affleck-Kennedy-Lieb-Tasaki (AKLT) model and its exact ground state or AKLT state [12]. The compact representation of the AKLT state [13] provided new insight into the Haldane phase. In addition, it was subsequently used in a variety of contexts for variational calculations on quantum spin systems [13,14].

The Kitaev honeycomb model (KHM) is an exactly soluble model which exhibits gapless and gapped Kitaev spin liquid (KSL) ground states with fractionalized excitations [15]. Recent successful realizations of Kitaev materials [16–22] triggered a burst of theoretical investigations on KHM and its extensions [23–25]. In addition, owing to the non-Abelian phase of the KSL driven by the magnetic field [26,27] and its potential application to quantum computation, it has been a subject of active research for the last decade. We refer the reader to Ref. [28] for an exhaustive list of relevant literature. Tensor network (TN) methods have been also employed to represent the KSL [29,30]. However, the Majorana basis TN requires a three-dimensional structure which makes it impractical as a tool for numerical optimization [29]. On the other hand, the spin basis TN study, which was done with computationally expensive optimization, suffers from an undesirable breaking of symmetries [30]. In this Letter, we provide a compact TN representation for the KHM that is defined with the spin basis and retains various symmetries.

Model.—The KHM is defined as [15]

$$\hat{\mathcal{H}} = -\sum_{\langle\alpha\beta\rangle_\gamma} J_\gamma \hat{\sigma}^\gamma_\alpha \hat{\sigma}^\gamma_\beta, \tag{1}$$

where $\langle\alpha\beta\rangle_\gamma$ stands for a pair on the $\gamma(=x,y,z)$ links connecting sites α and β, as depicted in Fig. 1(a). As demonstrated in Kitaev's seminal work [15], the Hamiltonian commutes with the so-called flux operators defined on all hexagonal plaquettes (p): $[\hat{\mathcal{H}}, \hat{W}_p] = 0$, with $\hat{W}_p = \hat{\sigma}^x_1\hat{\sigma}^y_2\hat{\sigma}^z_3\hat{\sigma}^x_4\hat{\sigma}^y_5\hat{\sigma}^z_6$, where the site indices 1–6 are as defined in Fig. 1(a). Therefore, the Hilbert space is sectorized by each flux number $\{\hat{W}_p = \pm 1\}$. Even further, in each sector, the KHM becomes a noninteracting Majorana fermion hopping model in the background of static Z_2 gauge fields. The ground states live in the vortex-free sector ($\hat{W}_p = +1$ for all p), and they form a critical KSL phase around the isotropic point ($J_x = J_y = J_z = \pm 1$). In this Letter, we consider only the isotropic point at which the KHM is invariant under the following symmetry transformations: $C_6\hat{U}_{C_6}$ and $\sigma\hat{U}_\sigma$, where $\hat{U}_{C_6} = \otimes_\alpha(\hat{\sigma}^0_\alpha + i\hat{\sigma}^x_\alpha + i\hat{\sigma}^y_\alpha + i\hat{\sigma}^z_\alpha)/2$, $\hat{U}_\sigma = \otimes_\alpha(\hat{\sigma}^x_\alpha - \hat{\sigma}^y_\alpha)/\sqrt{2}$, and C_6, σ, respectively, denote the 60° spatial rotation and inversion as depicted in Fig. 1(a). One can easily verify that $[C_6\hat{U}_{C_6}, \hat{\mathcal{H}}] = 0 = [\sigma\hat{U}_\sigma, \hat{\mathcal{H}}]$. Also, the KHM is invariant under the time-reversal and translational symmetries.

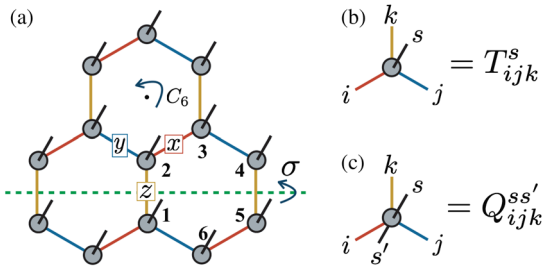

FIG. 1. Schematic figures of (a) the TPS setup on the honeycomb lattice, (b) its building block tensor T^s_{ijk}, and (c) a building block tensor $Q^{ss'}_{ijk}$ of the loop gas TPO defined in Eq. (2). Here, the x, y, and z links in the model [Eq. (1)] are characterized in red, blue, and yellow, respectively.

Tensor network representation.—We employ the tensor product state (TPS) representation [31]. Since the KSL is a zero-flux state [32], we reasonably assume the TPS to be translationally symmetric. Additionally, we assume that the tensor does not depend on the sublattice, and therefore our *Ansatz* is rewritten as $|\psi\rangle = t\mathrm{Tr}\prod_\alpha |T_{i_\alpha j_\alpha k_\alpha}\rangle$, where tTr stands for the tensor trace or contraction of all virtual indices $\{i_\alpha, j_\alpha, k_\alpha\}$, α labels the site, and $|T_{ijk}\rangle \equiv \sum_s T^s_{ijk}|s\rangle$, with s being the local quantum number. Its graphical illustration is presented in Fig. 1, where the black open leg denotes the physical degrees of freedom. In what follows, we will construct the local tensor $|T_{ijk}\rangle$ (we identify T^s_{ijk} and $|T_{ijk}\rangle$ and call both "tensor" hereafter) with consideration for the symmetries, the vortex-free condition, and the gauge structure. In the Letter, we discuss the ferromagnetic model ($J_\gamma = 1$) only since the antiferromagnetic one is a trivial generalization and is discussed in the Supplemental Material (SM) [33].

Zeroth order tensor.—We begin by introducing a bond dimension $D = 2$ tensor product operator (TPO) referred to as the *loop gas* (LG) operator, $\hat{Q}_{\mathrm{LG}} = t\mathrm{Tr}\prod_\alpha Q^{ss'}_{i_\alpha j_\alpha k_\alpha}|s\rangle\langle s'|$, with a building block tensor

$$Q^{ss'}_{ijk} = \tau_{ijk}[(\hat{\sigma}^x)^{1-i}(\hat{\sigma}^y)^{1-j}(\hat{\sigma}^z)^{1-k}]_{ss'}, \tag{2}$$

which is depicted in Fig. 1(c). The virtual indices i, j, and k range from 0 to 1 ($D = 2$), and nonzero elements of the τ tensor are $\tau_{000} = -i$ and $\tau_{011} = \tau_{101} = \tau_{110} = 1$. To simplify the notation, we define the local operator as $\hat{Q}_{ijk} = \sum_{s,s'} Q^{ss'}_{ijk}|s\rangle\langle s'|$. One can verify at the local tensor level that the LG operator respects the symmetries of the KHM. For instance, applying $C_6\hat{U}_{C_6}$ on the $\hat{Q}$ tensor leaves it intact, i.e.,

$$(C_6\hat{U}_{C_6})\hat{Q}_{ijk}(C_6\hat{U}_{C_6})^\dagger = \hat{Q}_{ijk}.$$

Here, we use the facts that the $\hat{U}_{C_6}$ transformation rotates the spin, i.e., $U_{C_6}\hat{\sigma}^{x,y,z}_\alpha U^\dagger_{C_6} = \hat{\sigma}^{z,x,y}_\alpha$, while the C_6 rotation permutes the virtual indices as follows: $C_6 \circ (ijk) = (kij)$. Therefore, the resulting LG operator is invariant under the $(C_6\hat{U}_{C_6})$ transformation, and other symmetries of the KHM can be shown in a similar way [33]. Note that the Q operator satisfies the following relation,

$$\begin{aligned}
\hat{\sigma}^x\hat{Q}_{ijk} &= v_{jj'}v^*_{kk'}\hat{Q}_{ij'k'},\\
\hat{\sigma}^y\hat{Q}_{ijk} &= v_{kk'}v^*_{ii'}\hat{Q}_{i'jk'},\\
\hat{\sigma}^z\hat{Q}_{ijk} &= v_{ii'}v^*_{jj'}\hat{Q}_{i'j'k},
\end{aligned} \tag{3}$$

with a matrix v, of which nonzero elements are $v_{01} = i$ and $v_{10} = 1$, acting on the virtual bonds. Repeated indices are summed over, except where explicitly stated otherwise. Using Eq. (3), one can verify a relation $\hat{W}_p\hat{Q}_{\mathrm{LG}} = \hat{Q}_{\mathrm{LG}}\hat{W}_p = \hat{Q}_{\mathrm{LG}}$. To be more specific, the invariance of a patch of $\hat{Q}_{\mathrm{LG}}$ under the action of $\hat{W}_p$ can be shown as follows:

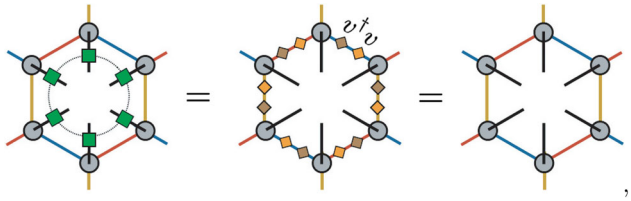

where the connected green squares denote $\hat{W}_p$, and a physical leg is omitted for simplicity. Here, Eq. (3) and $v^\dagger v = 1$ are used in the first and second equalities, respectively. This remarkable relation guarantees a quantum state $|\psi\rangle = \hat{Q}_{\mathrm{LG}}|\phi\rangle$, where $|\phi\rangle$ is an arbitrary state, being vortex-free and thus nonmagnetic. Notice that the LG operator is identical to the projector $\prod_p(1 + \hat{W}_p)/2$ up to a normalization factor.

Regarding the $(C_6\hat{U}_{C_6})$ symmetry, let us apply $\hat{Q}_{\mathrm{LG}}$ on a product state $|\phi_0\rangle = \otimes_\alpha |(111)\rangle_\alpha$, where $|(111)\rangle$ denotes a spin aligned along the (1,1,1) direction: $\langle(111)|\vec{\sigma}|(111)\rangle = (1,1,1)/\sqrt{3}$. Note that the *Ansatz* $|\phi_0\rangle$ is a classical ground state respecting the $(C_6\hat{U}_{C_6})$ symmetry. Now, we define a quantum state $|\psi_0\rangle \equiv \hat{Q}_{\mathrm{LG}}|\phi_0\rangle$ which consists of a building block tensor

$$|T^0_{ijk}\rangle \equiv \hat{Q}_{ijk}|(111)\rangle. \tag{4}$$

We refer to this as the *zeroth order tensor*. By virtue of the τ tensor in $\hat{Q}_{ijk}$, one can visualize the *Ansatz* $|\psi_0\rangle$ as follows:

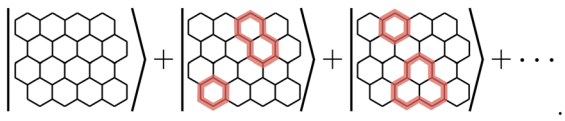

(5)

Here, the empty site stands for the $|(111)\rangle$ state, while the red loops denote the product of the $\hat{\sigma}^x|(111)\rangle$, $\hat{\sigma}^y|(111)\rangle$,

and $\hat{\sigma}^z|(111)\rangle$ states, depending on the direction of loop on each site.

By computing the norm of the LG *Ansatz*, we can show its criticality. To this end, we first note that the LG operator is Hermitian as well as idempotent [33]: $\hat{Q}_{\mathrm{LG}}^{\dagger}\hat{Q}_{\mathrm{LG}} = N_\Gamma \hat{Q}_{\mathrm{LG}}$, where N_Γ is the total number of the loop configuration in the system. Using such properties and a simple identity $\langle(111)|\hat{\sigma}^\gamma|(111)\rangle = 1/\sqrt{3}$, it is straightforward to show that the norm of $|\psi_0\rangle$ reads

$$\langle\psi_0|\psi_0\rangle = N_\Gamma \sum_{G\in\Gamma}\left(\frac{1}{\sqrt{3}}\right)^{l_G} = N_\Gamma \times Z_{O(1)}\left(\frac{1}{\sqrt{3}}\right), \quad (6)$$

where Γ denotes the set of all possible loop configurations and l_G is the total length of loops in a configuration G. Also, $Z_{O(1)}(x)$ stands for the partition function of the classical $O(1)$ loop gas model with the fugacity x, which is exactly solvable and critical at $x_c = 1/\sqrt{3}$ [34]. It indicates that the norm of $|\psi_0\rangle$ is exactly mapped onto the partition function of the critical classical model, which guarantees the criticality of $|\psi_0\rangle$ [35]. In addition, the Ising conformal field theory (CFT) with the central charge $c = 1/2$ is known to characterize the critical LG model [34], which is consistent with the KSL of the KHM [36–38].

The LG structure encoded in the τ tensor is useful in describing the vortex excitation of the KSL. To see this, we first note that the τ tensor is invariant under a gauge transformation $g = \hat{\sigma}^z$, i.e., $g_{ii'}g_{jj'}g_{kk'}\tau_{i'j'k'} = \tau_{ijk}$, and thus

$$g_{ii'}g_{jj'}g_{kk'}|T^0_{i'j'k'}\rangle = |T^0_{ijk}\rangle.$$

With the trivial gauge transformation I_2 being a two-dimensional identity matrix, g forms a Z_2 invariant gauge group (IGG). The stringlike action of g on the links would twist the gauge fields [15] along the string and hence create two vortices $\hat{W}_p = -1$ at both ends, as demonstrated below:

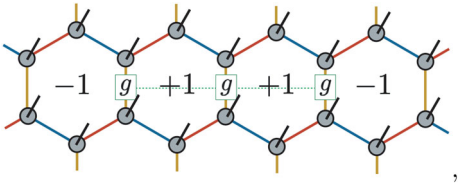

where ± 1 in the hexagon denotes $\hat{W}_p$. One can explicitly show [33] such a creation and move of fluxes using Eq. (3).

Finally, we measure the KHM energy (per bond) of $|\psi_0\rangle$ and obtain $E = -0.16349$, which is rather higher than the exact one $E_{\mathrm{Kitaev}} \simeq -0.19682$ [15]. Details on numerics will be discussed later. By construction, the LG *Ansatz* $|\psi_0\rangle$ made of the zeroth order tensor satisfies most of the physical constraints respected in the KSL (see the SM [33] for the time-reversal and $\sigma\hat{U}_\sigma$ symmetries) but is energetically far away from the exact solution. In what follows, we present a simple but effective TPO ($D = 2$) applied to the LG *Ansatz* which reduces the energy greatly without violating the constraints. We refer to it as the *dimer gas* (DG) operator.

Higher order tensors.—The DG operator is defined by $\hat{R}_{\mathrm{DG}} = t\mathrm{Tr}\prod_\alpha \hat{R}_{i_\alpha j_\alpha k_\alpha}$ with

$$\hat{R}_{ijk} = \zeta_{ijk}(\hat{\sigma}^x)^i(\hat{\sigma}^y)^j(\hat{\sigma}^z)^k. \quad (7)$$

Here, nonzero elements of the ζ tensor are $\zeta_{000} = 1$ and $\zeta_{100} = \zeta_{010} = \zeta_{001} = z$ with $i, j, k = 0, 1$, and z is a real (or pure imaginary) variational parameter fixing the fugacity of a dimer. In this context, the dimer denotes the operator $\hat{\mathcal{H}}^\gamma_{\alpha\beta}$. Then, the DG operator can be interpreted as the sum of all possible dimer configurations, i.e., $\hat{R}_{\mathrm{DG}}(z) = \sum_{G\in\Gamma_D}\hat{R}_G(z)$, where $\hat{R}_G(z) = \otimes_{\langle\alpha\beta\rangle_\gamma\in G}(z\hat{\mathcal{H}}^\gamma_{\alpha\beta})$ is defined for each dimer configuration G, and Γ_D is the set of all dimer configurations:

$\Gamma_{\mathrm{D}} =$ 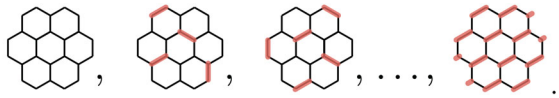 . (8)

Because $[\hat{\mathcal{H}}^\gamma_{\alpha\beta}, \hat{W}_p] = 0$, it is obvious that $\hat{R}_G$ commutes with $\hat{W}_p$ for any G, and hence $\hat{R}_{\mathrm{DG}}$ does: $[\hat{R}_{\mathrm{DG}}, \hat{W}_p] = 0$. In fact, we can easily prove that $[\hat{R}_{\mathrm{DG}}, \hat{Q}_{\mathrm{LG}}] = 0$ and that the DG operator respects all symmetries of the KSL [33]. Therefore, its multiplication to $|\psi_0\rangle$ does not contaminate the features of the KSL, regardless of z. Moreover, it can be expressed as the polynomial function of the KHM Hamiltonian, which may be the reason why it improves the energy of the *Ansatz* quite efficiently. The first key observation is that we can graphically represent Eq. (1) raised to the nth power as the linear combination of elements of Γ_D as

$\mathcal{H}^N = \alpha_0$ 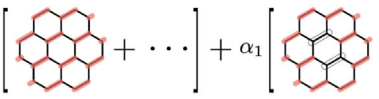 $+ \alpha_1$ 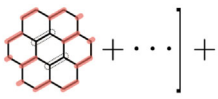 $+ \cdots$

$+ \beta$ 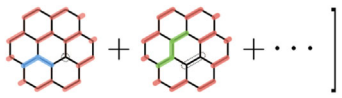

Here, the number of sites in the system is assumed to be $2N$. The terms grouped with a coefficient α_0 are the fully packed configurations, while the second ones are the configuration with $N - 2$ dimers. The terms on the second line have q-mers longer than a dimer, e.g., trimer $\hat{\mathcal{H}}^x_{\alpha\beta}\hat{\mathcal{H}}^y_{\beta\gamma}$. All of those terms with q-mers are canceled by the anticommutativity of the Pauli matrices, and thus $\beta = 0$. Note that the configurations with the same number of

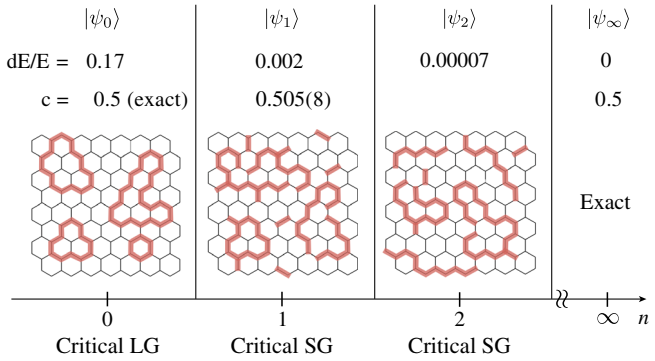

FIG. 2. Overview of the nth order *Ansatz* $|\psi_n\rangle$ obtained by LG and DG operators, where SG denotes the string gas, $dE = E - E_{\text{Kitaev}}$ denotes the energy deviation, and c stands for the central charge.

dimers share the coefficient which resembles the $\hat{R}_{\text{DG}}$. Then, one can recast it as $\hat{R}_{\text{DG}} = \sum_M h_M \hat{\mathcal{H}}^{N-2M}$ with proper coefficients h_M. Note that our approach is not a perturbative one [39].

Now, we define the nth order *Ansatz* as $|\psi_n(\{z_i\})\rangle = \prod_{i=1}^{n} \hat{R}_{\text{DG}}(z_i)|\psi_0\rangle$ having n complex variational parameters. Owing to the application of the DG operator, the *Ansatz* $|\psi_n\rangle$ can be interpreted as a *string gas* state which is a linear superposition of *string* configurations. The string configuration consists of open and closed strings, connected loops, and string-connected loops, as depicted in Fig. 2. The building block tensor of $|\psi_n\rangle$, referred to as the nth order tensor, is obtained by applying the $\hat{R}_{ijk}$ operator n times on the zeroth order tensor in Eq. (4). The bond dimension scales as $D = 2^{n+1}$. Note that the LG feature or the τ tensor in the zeroth tensor is inherited by all higher order tensors. Furthermore, the $\hat{R}_{ijk}$ operator is invariant only under the trivial gauge transformation, and thus its action does not enlarge the Z_2 IGG, of which the nontrivial element is simply $g_n = I_{2^n} \otimes \hat{\sigma}^z$. In contrast to the zeroth order case, the norm of $|\psi_n\rangle$ does not map onto the LG model. However, by employing the loop TN renormalization [40], we numerically prove that the nth order *Ansätze* are also critical and are characterized by the Ising CFT as summarized in Fig. 2. We also present the best variational energies at each order in Fig. 2, and the details are given below.

Variational Ansatz.—Now, we turn on and tune variational parameters to obtain a better *Ansatz* than the zeroth one. We parametrize the ζ tensor as follows: $\zeta_{000} = \cos\phi$, $\zeta_{100} = \zeta_{010} = \zeta_{001} = \sin\phi$, and hence $\hat{R}_{ijk}(z) \to \hat{R}_{ijk}(\phi)$. For measuring the energy, we employ the corner transfer matrix renormalization group method (CTMRG) [41–43], whose accuracy is controlled by the dimension χ of the CTM. The parallel C++ library MPTENSOR [44] is utilized to perform the CTMRG.

Let us begin with the first order *Ansatz* $|\psi_1(\phi)\rangle$ and its building block tensor

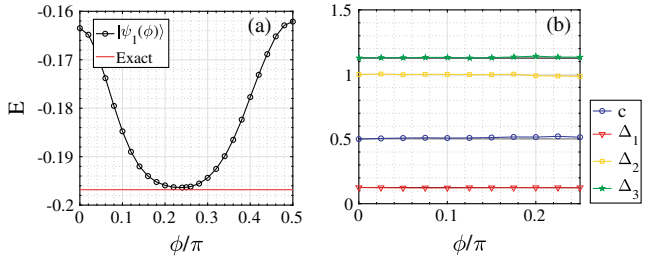

FIG. 3. (a) Energy of $|\psi_1(\phi)\rangle$, whose building block tensor is defined in Eq. (9), and (b) the central charge c and scaling dimensions (Δ_i) as a function of ϕ. The black solid lines in (b) denote the exact c and Δ_i from the Ising universality class.

$$|T^1_{i_1 j_1 k_1}(\phi)\rangle = \hat{R}_{ijk}(\phi)|T^0_{i_0 j_0 k_0}\rangle, \tag{9}$$

where $i_n = 2^n i + i_{n-1}$ and $i = 0, 1$. The energy of $|\psi_1(\phi)\rangle$ is presented in Fig. 3(a) as a function of ϕ, where the lowest value, $E = -0.19644$, is found at $\phi = 0.24\pi$. Here, we fix $\chi = 64$. It is remarkable that the first order tensor ($D = 4$) already attains such a small error of 0.2%. Furthermore, we perform the loop TN renormalization to evaluate the norm of $|\psi_1(\phi)\rangle$ and extract the central charge and scaling dimensions presented in Fig. 3(b) [see the SM [33] for more details]. All of those are in excellent agreement with the ones Ising CFT, and therefore our *Ansätze* are critical and belong to the same universality class. To obtain an *Ansatz* even closer to the KSL, we consider the second order *Ansatz* $|\psi_2\rangle$ and tensor ($D = 8$):

$$|T^2_{i_2 j_2 k_2}(\phi,\theta)\rangle = \hat{R}_{ijk}(\theta)|T^1_{i_1 j_1 k_1}(\phi)\rangle. \tag{10}$$

Its overall energy landscape is shown in Fig. 4(a) as functions of (ϕ,θ) and is minimized at $(\phi,\theta) = (0.342\pi, 0.176\pi)$. After an additional scaling with respect to χ [33], we obtain the best variational *Ansatz* with $E = -0.19681$, which is only 0.007% higher than the exact one. Also, using the environment tensors [45], the five largest correlation lengths (ξ_i) are extracted and shown in Fig. 4(b), which are diverging with χ. An analogous figure is shown for ψ_1 in the SM [33]. Therefore, we

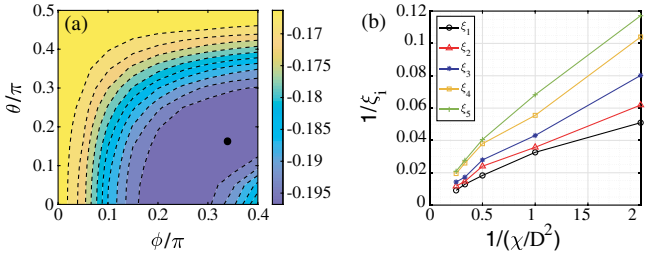

FIG. 4. (a) Energy landscape of $|\psi_2(\phi,\theta)\rangle$ constructed by the tensor in Eq. (10) as functions of ϕ and θ. The energy minimum is denoted by the black dot, at which the variational energy is $E = -0.19681$ [33]. (b) The five largest correlation lengths ξ_i of the best *Ansatz* represented by the dot in (a), where χ stands for the bond dimension of CTMRG.

reasonably conclude that the *Ansätze* made of higher order tensors form a family of gapless states which we believe are smoothly connected to the exact KSL and, as a series, converge to it.

Further, we found [33] that applying the (111)-direction magnetic field drives the *Ansätze* into the gapped phase [15]. We speculate that these gapped *Ansätze* host non-Abelian anyonic excitations. The description of the non-Abelian and Abelian topological phases under the LG and SG schemes is an interesting problem, and now further study is in progress [46].

Conclusion.—Based on the physical and gauge symmetries and the vortex-free condition, we have constructed a compact TN representation which generates a family of KSL-like states sharing the features of the KHM ground state. In this sense, the *Ansätze* given in this Letter are analogous to the AKLT state as a member of the Haldane states, or the RVB state as an *Ansatz* of frustrated quantum magnets [4,12]. Under this scheme, the string gas structure of the KSL comes into sight clearly, which offers a novel viewpoint for the KSL and its physics. It also provides an intuitive picture for the KSL in the *spin* language without referring to the Majorana fermion, which has never been provided before. There are many generalizations that one can envision, as well as concrete open questions involving the LG and SG *Ansätze*, e.g., general LGs having larger internal degrees of freedom and their parent Hamiltonians. The relation between the general LGs and the string-net states [47] is another interesting issue to explore. We also find that the *Ansatz* discussed in this Letter provides a good initial state for a variational method for the KHM with the magnetic field [48]. Further, for the anisotropic KHM, one can choose an initial magnetic state which differs from the state $|(111)\rangle$ and introduce a bond-dependent dimer fugacity as additional variational parameters to optimize the model [46]. Therefore, we expect our work could furnish a better understanding of KSL and its neighboring phases observed in Kitaev quantum magnets such as α-$RuCl_3$ [20,49] and studied theoretically in extended KHMs [17,22,23,25,50]. Using two variational parameters, an accuracy of 0.007% in energy is obtained, which has never been achieved by other numerical optimizations [51–53]. This high accuracy, together with the observed systematic convergence, leads us to believe that the present scheme not only correctly captures the essence of KSL physics but also provides a new direction for quantitatively accurate descriptions of quantum spin liquids.

The computation in this work was executed on computers at the Supercomputer Center, ISSP, University of Tokyo, and also on the K computer (Project ID No. hp190196). N. K.'s work is funded by the ImPACT Program of Council for Science, Technology and Innovation (Cabinet Office, Government of Japan). H.-Y. L. was supported by MEXT as "Exploratory Challenge on Post-K Computer" (Frontiers of Basic Science: Challenging the Limits). R. K. and T. O. were supported by MEXT as "Priority Issue on Post-K Computer" (Creation of New Functional Devices and High-Performance Materials to Support Next-Generation Industries), and JSPS KAKENHI Grant No. 15K17701, respectively.

*kawashima@issp.u-tokyo.ac.jp

[1] L. Savary and L. Balents, Quantum spin liquids: A review, Rep. Prog. Phys. **80**, 016502 (2017).
[2] P. W. Anderson, The resonating valence bond state in La_2CuO_4 and superconductivity, Science **235**, 1196 (1987).
[3] R. Moessner and S. L. Sondhi, Resonating Valence Bond Phase in the Triangular Lattice Quantum Dimer Model, Phys. Rev. Lett. **86**, 1881 (2001).
[4] X.-G. Wen, Quantum orders and symmetric spin liquids, Phys. Rev. B **65**, 165113 (2002).
[5] Y. Zhou, K. Kanoda, and T.-K. Ng, Quantum spin liquid states, Rev. Mod. Phys. **89**, 025003 (2017).
[6] D. Poilblanc, N. Schuch, D. Pérez-García, and J. Ignacio Cirac, Topological and entanglement properties of resonating valence bond wave functions, Phys. Rev. B **86**, 014404 (2012).
[7] H. Lee, Y.-t. Oh, J. H. Han, and H. Katsura, Resonating valence bond states with trimer motifs, Phys. Rev. B **95**, 060413(R) (2017).
[8] R. Kaneko, S. Morita, and M. Imada, Gapless spin-liquid phase in an extended spin 1/2 triangular Heisenberg model, J. Phys. Soc. Jpn. **83**, 093707 (2014).
[9] S. Jiang, P. Kim, J. H. Han, and Y. Ran, Competing spin liquid phases in the $S = 1/2$ Heisenberg model on the Kagome lattice, SciPost Phys. **7**, 006 (2019).
[10] Y. Iqbal, W.-J. Hu, R. Thomale, D. Poilblanc, and F. Becca, Spin liquid nature in the Heisenberg $J_1 - J_2$ triangular antiferromagnet, Phys. Rev. B **93**, 144411 (2016).
[11] J.-W. Mei, J.-Y. Chen, H. He, and X.-G. Wen, Gapped spin liquid with $\mathbb{z}_2$ topological order for the Kagome Heisenberg model, Phys. Rev. B **95**, 235107 (2017).
[12] I. Affleck, T. Kennedy, E. H. Lieb, and H. Tasaki, Rigorous Results on Valence-Bond Ground States in Antiferromagnets, Phys. Rev. Lett. **59**, 799 (1987).
[13] A. Klümper, A. Schadschneider, and J. Zittartz, Matrix product ground states for one-dimensional spin-1 quantum antiferromagnets, Europhys. Lett. **24**, 293 (1993).
[14] A. K. Kolezhuk and H.-J. Mikeska, Non-Haldane Spin-Liquid Models with Exact Ground States, Phys. Rev. Lett. **80**, 2709 (1998).
[15] A. Kitaev, Anyons in an exactly solved model and beyond, Ann. Phys. (Amsterdam) **321**, 2 (2006).
[16] G. Khaliullin, Orbital order and fluctuations in Mott insulators, Prog. Theor. Phys. Suppl. **160**, 155 (2005).
[17] G. Jackeli and G. Khaliullin, Mott Insulators in the Strong Spin-Orbit Coupling Limit: From Heisenberg to a Quantum Compass and Kitaev Models, Phys. Rev. Lett. **102**, 017205 (2009).
[18] K. W. Plumb, J. P. Clancy, L. J. Sandilands, V. Vijay Shankar, Y. F. Hu, K. S. Burch, H.-Y. Kee, and Y.-J. Kim, α-$RuCl_3$: A spin-orbit assisted Mott insulator on a honeycomb lattice, Phys. Rev. B **90**, 041112(R) (2014).

[19] X. Zhou, H. Li, J. A. Waugh, S. Parham, H.-S. Kim, J. A. Sears, A. Gomes, H.-Y. Kee, Y.-J. Kim, and D. S. Dessau, Angle-resolved photoemission study of the Kitaev candidate α-$RuCl_3$, Phys. Rev. B **94**, 161106(R) (2016).

[20] A. Banerjee, C. A. Bridges, J.-Q. Yan, A. A. Aczel, L. Li, M. B. Stone, G. E. Granroth, M. D. Lumsden, Y. Yiu, Johannes Knolle *et al.*, Proximate Kitaev quantum spin liquid behaviour in a honeycomb magnet, Nat. Mater. **15**, 733 (2016).

[21] S. Trebst, Kitaev materials, arXiv:1701.07056.

[22] Y. Singh and P. Gegenwart, Antiferromagnetic Mott insulating state in single crystals of the honeycomb lattice material Na_2IrO_3, Phys. Rev. B **82**, 064412 (2010).

[23] I. Kimchi and Y.-Z. You, Kitaev-Heisenberg-$J_2 - J_3$ model for the iridates A_2IrO_3, Phys. Rev. B **84**, 180407(R) (2011).

[24] A. Catuneanu, Y. Yamaji, G. Wachtel, Y. B. Kim, and H.-Y. Kee, Path to stable quantum spin liquids in spin-orbit coupled correlated materials, npj Quantum Mater. **3**, 23 (2018).

[25] M. Gohlke, G. Wachtel, Y. Yamaji, F. Pollmann, and Y. B. Kim, Quantum spin liquid signatures in Kitaev-like frustrated magnets, Phys. Rev. B **97**, 075126 (2018).

[26] H.-C. Jiang, Z.-C. Gu, X.-L. Qi, and S. Trebst, Possible proximity of the Mott insulating iridate Na_2IrO_3 to a topological phase: Phase diagram of the Heisenberg-Kitaev model in a magnetic field, Phys. Rev. B **83**, 245104 (2011).

[27] Z. Zhu, I. Kimchi, D. N. Sheng, and L. Fu, Robust non-Abelian spin liquid and a possible intermediate phase in the antiferromagnetic Kitaev model with magnetic field, Phys. Rev. B **97**, 241110(R) (2018).

[28] C. Nayak, S. H. Simon, A. Stern, M. Freedman, and S. D. Sarma, Non-Abelian anyons and topological quantum computation, Rev. Mod. Phys. **80**, 1083 (2008).

[29] P. Schmoll and R. Orús, Kitaev honeycomb tensor networks: Exact unitary circuits and applications, Phys. Rev. B **95**, 045112 (2017).

[30] J. O. Iregui, P. Corboz, and M. Troyer, Probing the stability of the spin-liquid phases in the Kitaev-Heisenberg model using tensor network algorithms, Phys. Rev. B **90**, 195102 (2014).

[31] F. Verstraete, V. Murg, and J. I. Cirac, Matrix product states, projected entangled pair states, and variational renormalization group methods for quantum spin systems, Adv. Phys. **57**, 143 (2008).

[32] Y.-Z. You, I. Kimchi, and A. Vishwanath, Doping a spin-orbit Mott insulator: Topological superconductivity from the Kitaev-Heisenberg model and possible application to $(Na_2/Li_2)IrO_3$, Phys. Rev. B **86**, 085145 (2012).

[33] See Supplemental Material at http://link.aps.org/supplemental/10.1103/PhysRevLett.123.087203 for details omitted from the main text.

[34] B. Nienhuis, Exact Critical Point and Critical Exponents of $O(n)$ Models in Two Dimensions, Phys. Rev. Lett. **49**, 1062 (1982).

[35] E. Ardonne, P. Fendley, and E. Fradkin, Topological order and conformal quantum critical points, Ann. Phys. (Amsterdam) **310**, 493 (2004).

[36] T. Månsson, V. Lahtinen, J. Suorsa, and E. Ardonne, Condensate-induced transitions and critical spin chains, Phys. Rev. B **88**, 041403(R) (2013).

[37] V. Lahtinen, T. Månsson, and E. Ardonne, Hierarchy of exactly solvable spin-1/2 chains with $so(N)_1$ critical points, Phys. Rev. B **89**, 014409 (2014).

[38] K. Meichanetzidis, M. Cirio, J. K. Pachos, and V. Lahtinen, Anatomy of fermionic entanglement and criticality in Kitaev spin liquids, Phys. Rev. B **94**, 115158 (2016).

[39] L. Vanderstraeten, M. Mariën, J. Haegeman, N. Schuch, J. Vidal, and F. Verstraete, Bridging Perturbative Expansions with Tensor Networks, Phys. Rev. Lett. **119**, 070401 (2017).

[40] S. Yang, Z.-C. Gu, and X.-G. Wen, Loop Optimization for Tensor Network Renormalization, Phys. Rev. Lett. **118**, 110504 (2017).

[41] T. Nishino and K. Okunishi, Corner transfer matrix renormalization group method, J. Phys. Soc. Jpn. **65**, 891 (1996).

[42] R. Orús and G. Vidal, Simulation of two-dimensional quantum systems on an infinite lattice revisited: Corner transfer matrix for tensor contraction, Phys. Rev. B **80**, 094403 (2009).

[43] P. Corboz, J. Jordan, and G. Vidal, Simulation of fermionic lattice models in two dimensions with projected entangled-pair states: Next-nearest neighbor Hamiltonians, Phys. Rev. B **82**, 245119 (2010).

[44] S. Morita *et al.*, MPTENSOR: Parallel library for tensor network method, 2016.

[45] H.-Y. Lee and N. Kawashima, Spin-one bilinear-biquadratic model on a star lattice, Phys. Rev. B **97**, 205123 (2018).

[46] H.-Y. Lee, R. Kaneko, T. Okubo, and N. Kawashima, Abelian and non-abelian chiral spin liquids in a compact tensor network representation, arXiv:1907.02268.

[47] P. Fendley, Topological order from quantum loops and nets, Ann. Phys. (Amsterdam) **323**, 3113 (2008).

[48] R. Kaneko, T. Okubo, H.-Y. Lee, Y. Yamaji, and N. Kawashima (to be published).

[49] A. Banerjee, P. Lampen-Kelley, J. Knolle, C. Balz, A. A. Aczel, B. Winn, Y. Liu, D. Pajerowski, J. Yan, C. A. Bridges *et al.*, Excitations in the field-induced quantum spin liquid state of α-$RuCl_3$, npj Quantum Mater. **3**, 8 (2018).

[50] J. Chaloupka, G. Jackeli, and G. Khaliullin, Kitaev-Heisenberg Model on a Honeycomb Lattice: Possible Exotic Phases in Iridium Oxides A_2IrO_3, Phys. Rev. Lett. **105**, 027204 (2010).

[51] H. N. Phien, J. A. Bengua, H. D. Tuan, P. Corboz, and R. Orús, Infinite projected entangled pair states algorithm improved: Fast full update and gauge fixing, Phys. Rev. B **92**, 035142 (2015).

[52] P. Corboz, Variational optimization with infinite projected entangled-pair states, Phys. Rev. B **94**, 035133 (2016).

[53] L. Vanderstraeten, J. Haegeman, P. Corboz, and F. Verstraete, Gradient methods for variational optimization of projected entangled-pair states, Phys. Rev. B **94**, 155123 (2016).